Liquid Crystals
Publication details, including instructions for authors and subscription information:
http://www.informaworld.com/smpp/title~content=t713926090

Continuum modelling of hybrid-aligned nematic liquid crystal cells: optical response and flexoelectricity-induced voltage shift

N. T. Kirkman[a]; T. Stirner Corresponding author[a]; W. E. Hagston[a]
[a] Department of Physics, University of Hull, Hull HU6 7RX, UK

Online publication date: 19 May 2010

To cite this Article Kirkman, N. T. , Stirner Corresponding author, T. and Hagston, W. E.(2003) 'Continuum modelling of hybrid-aligned nematic liquid crystal cells: optical response and flexoelectricity-induced voltage shift', Liquid Crystals, 30: 9, 1115 — 1122
To link to this Article: DOI: 10.1080/02678290310001594562
URL: http://dx.doi.org/10.1080/02678290310001594562

LIQUID CRYSTALS, VOL. 30, NO. 9, SEPTEMBER, 2003, 1115–1122

Taylor & Francis
Taylor & Francis Group

Continuum modelling of hybrid-aligned nematic liquid crystal cells: optical response and flexoelectricity-induced voltage shift

N. T. KIRKMAN, T. STIRNER* and W. E. HAGSTON
Department of Physics, University of Hull, Hull HU6 7RX, UK

(*Received 21 November 2002; in final form 19 March 2003; accepted 12 May 2003*)

A continuum model is employed to study systematically the optical response of hybrid-aligned nematic (HAN) liquid crystal cells under the application of an external electric field. The influence of the flexoelectric effect is discussed for a large range of anchoring strengths at the homeotropic alignment layer. It is shown that the optical response of HAN cells is governed by a complicated interplay between the flexoelectric coefficient and homeotropic anchoring strength. In particular, the calculations reveal that, for weak homeotropic anchoring, the flexoelectric effect leads to a non-linear voltage shift of the optical transmittance as a function of flexoelectric coefficient, and gives rise to an asymmetry in the transmittance–voltage curve. Finally, a comparison of the continuum-model simulations with recent experimental observations indicates that both the flexoelectric coefficient and the anchoring strength of the nematic liquid crystal MBBA on a homeotropic polyimide alignment layer are significantly lower than previously reported.

1. Introduction

At present, liquid crystal displays (LCDs) represent the dominant flat panel device technology [1]. Twisted nematic LCDs are used primarily for low information-content applications such as calculators and digital watches, whereas supertwisted nematic LCDs are used in high information-content applications such as laptop computers. Recently, there has been increased interest in alternative LCD technologies. Amongst them are nematic displays which utilize a linear electro-optic effect [2–5]. This *flexoelectric* effect originates from a polarization of the nematic liquid crystal induced by splay or bend deformations. The flexoelectric polarization P is given as

$$P = e_{11}(\nabla\cdot\mathbf{n})\cdot\mathbf{n} + e_{33}(\nabla\times\mathbf{n})\times\mathbf{n} \qquad (1)$$

where e_{11} and e_{33} are the flexoelectric coefficients corresponding to splay and bend distortion of the nematic director field $\mathbf{n}$, respectively.

One type of liquid crystal cell which has both splay and bend distortions in its initial state is the hybrid-aligned nematic (HAN) cell [6–9]. This cell is characterized by homeotropic molecular alignment at one surface and homogeneous alignment at the other; it can be used (in conjunction with continuum modelling) to determine the flexoelectric coefficients of nematic liquid crystals. Various methods have been employed for the experimental characterization of HAN cells. Amongst them are measurements of the retardation of normally transmitted light [2, 3, 8], a pyroelectric technique [10, 11] and a leaky waveguide method [12–14]. Recently, Takahashi *et al.* [2] proposed a novel measurement method for flexoelectric coefficients that involves the fitting of the observed voltage shift in the optical transmittance of the HAN cell with numerical simulations. The aim of the present study is a systematic, theoretical investigation of the optical response of HAN cells using continuum theory [15]. As will be shown, the calculated voltage shift in the optical transmittance depends strongly on the homeotropic anchoring strength and is a complicated, non-linear function of the flexoelectric coefficient for weak homeotropic anchoring. Consequently, we will reconsider the experimental data of Takahashi *et al.* by fitting the entire optical response of the HAN cell with numerical simulations. This fitting procedure gives values for the flexoelectric coefficient and the homeotropic anchoring coefficient which are considerably smaller than those reported by Takahashi *et al.* [2].

*Author for correspondence; e-mail: t.stirner@hull.ac.uk

2. Theory

In the present paper we consider a HAN cell with the electric field applied along the cell normal (z direction). For the optical experiments described later, we can ignore the azimuthal angle of the director and simply describe the director field by the tilt angle $\Theta(z)$, i.e. the angle between the director and the surface (xy) plane.

Liquid Crystals ISSN 0267-8292 print/ISSN 1366-5855 online © 2003 Taylor & Francis Ltd
http://www.tandf.co.uk/journals
DOI: 10.1080/0267829031000159456 2

Following the notation of Takahashi *et al.* [2], the free energy density f_z can be written as

$$f_z = \frac{1}{2}f_{\text{elas}}(\Theta)\left(\frac{\partial\Theta}{\partial z}\right)^2 - \frac{1}{2}f_{\text{diel}}(\Theta)\left(\frac{\partial\varphi}{\partial z}\right)^2 + f_{\text{flex}}(\Theta)\left(\frac{\partial\Theta}{\partial z}\right)\left(\frac{\partial\varphi}{\partial z}\right) \tag{2}$$

where the three terms containing

$$f_{\text{elas}}(\Theta) = K_{11}\cos^2\Theta + K_{33}\sin^2\Theta$$
$$f_{\text{diel}}(\Theta) = \varepsilon_0\left(\Delta\varepsilon\sin^2\Theta + \varepsilon_{\text{n}}\right)$$

and

$$f_{\text{flex}}(\Theta) = (e_{11} + e_{33})\sin\Theta\cos\Theta$$

describe the elastic, dielectric and flexoelectric contributions to the free energy density, respectively. K_{11} (K_{33}) is the elastic constant for splay (bend) distortion, $\Delta\varepsilon(=\varepsilon_{\text{p}}-\varepsilon_{\text{n}})$ is the dielectric anisotropy, e_{11} (e_{33}) is the flexoelectric coefficient for splay (bend) distortion and $\varphi(z)$ is the electric scalar potential. Here we do not take into account the effects of a bulk charge distribution [6] or surface polarization [9, 13] since, in the experiments of interest to the present work, the effects of ionic screening were relatively small [2], and surface polarization effects have been shown to be of importance only for extremely low anchoring energies [6].

The evaluation of the director profile involves the minimization of the total free energy with respect to both Θ and φ. The resulting Euler–Lagrange equations can be written as

$$f'_{\text{elas}}(\Theta)\left(\frac{\partial\Theta}{\partial z}\right)^2 + 2f_{\text{elas}}(\Theta)\left(\frac{\partial^2\Theta}{\partial z^2}\right) + f'_{\text{diel}}(\Theta)\left(\frac{\partial\varphi}{\partial z}\right)^2 + 2f_{\text{flex}}(\Theta)\left(\frac{\partial^2\varphi}{\partial z^2}\right) = 0 \tag{3}$$

for minimization of the free energy with respect to Θ, and

$$f'_{\text{diel}}(\Theta)\left(\frac{\partial\Theta}{\partial z}\right)\left(\frac{\partial\varphi}{\partial z}\right) + f_{\text{diel}}(\Theta)\left(\frac{\partial^2\varphi}{\partial z^2}\right) - f'_{\text{flex}}(\Theta)\left(\frac{\partial\Theta}{\partial z}\right)^2 - f_{\text{flex}}(\Theta)\left(\frac{\partial^2\Theta}{\partial z^2}\right) = 0 \tag{4}$$

for minimization of the free energy with respect to φ.

Usually equations (3) and (4) are solved self-consistently [2, 6] with respect to both the director profile and the electric potential profile. We do not follow this procedure here. Instead, after rewriting equation (4) in the form

$$\frac{\mathrm{d}}{\mathrm{d}z}\left[f_{\text{diel}}(\Theta)\left(\frac{\partial\varphi}{\partial z}\right) - f_{\text{flex}}(\Theta)\left(\frac{\partial\Theta}{\partial z}\right)\right] = 0 \tag{5}$$

i.e.

$$f_{\text{diel}}(\Theta)\left(\frac{\partial\varphi}{\partial z}\right) - f_{\text{flex}}(\Theta)\left(\frac{\partial\Theta}{\partial z}\right) = const. \tag{6}$$

we solve the two coupled equations (3) and (6) by a straightforward numerical integration (employing the finite differences method) subject to the boundary conditions at both surfaces. The latter involve the surface free energy densities, f_{s}, at $z=0$ and $z=d$ which can be expressed in the Rapini–Papoular form, i.e.

$$f_{\text{s0}} = \frac{1}{2}A_{\Theta_0}\sin^2\left(\Theta_{[0]} - \Theta_0\right) \tag{7}$$

and

$$f_{\text{sd}} = \frac{1}{2}A_{\Theta_d}\sin^2\left(\Theta_{[d]} - \Theta_d\right) \tag{8}$$

respectively, where Θ_0 and Θ_d describe the angle of the easy axis on each surface, $\Theta_{[0]}$ and $\Theta_{[d]}$ describe the actual angle of the director, and A_{Θ_0} and A_{Θ_d} are the anchoring coefficients. Hence (by integrating from the homeotropic to the homogeneous alignment layer), the boundary conditions can be expressed as

$$f_{\text{elas}}\left(\Theta_{[0]}\right)\left.\frac{\partial\Theta}{\partial z}\right|_{z=0} + f_{\text{flex}}\left(\Theta_{[0]}\right)\left.\frac{\partial\varphi}{\partial z}\right|_{z=0} - \frac{1}{2}A_{\Theta_0}\sin\left[2\left(\Theta_{[0]} - \Theta_0\right)\right] = 0 \tag{9}$$

and

$$f_{\text{elas}}\left(\Theta_{[d]}\right)\left.\frac{\partial\Theta}{\partial z}\right|_{z=d} + f_{\text{flex}}\left(\Theta_{[d]}\right)\left.\frac{\partial\varphi}{\partial z}\right|_{z=d} + \frac{1}{2}A_{\Theta_d}\sin\left[2\left(\Theta_{[d]} - \Theta_d\right)\right] = 0 \tag{10}$$

at the two surfaces, respectively.

The applied voltage V can be calculated as [2, 15]

$$V = \int_0^d \left(\frac{\partial\varphi}{\partial z}\right)\mathrm{d}z \tag{11}$$

and the optical transmittance T can be written as [3]

$$T = \frac{1-\cos\Delta\phi}{2} \tag{12}$$

where the optical phase difference of the cell, $\Delta\phi$, is given by

$$\Delta\phi = \frac{2\pi}{\lambda}\int_0^d \left[n_{\text{eff}}(z) - n_{\text{o}}\right]\mathrm{d}z. \tag{13}$$

Here $n_{\text{eff}}(z) = n_{\text{o}}\left[1 - R\cos^2\Theta(z)\right]^{-\frac{1}{2}}$ with $\mathrm{R} = \left(n_{\text{e}}^2 - n_{\text{o}}^2\right)/n_{\text{e}}^2$. The wavelength of the incident light is denoted by λ, and n_{e} and n_{o} are the extraordinary and ordinary refractive indices of the nematic liquid crystal, respectively.

Table 1. Material parameters for MBBA and cell parameters employed in the calculations (unless stated otherwise).

Parameter	Value	Reference
$K_{11}/10^{-11}$ N	0.64	[2]
$K_{33}/10^{-11}$ N	0.82	[2]
ε_p	4.7	[6]
ε_n	5.4	[6]
n_e	1.80	[6]
n_o	1.57	[6]
$e/10^{-11}$ C m^{-1}	−5.0	
Θ_0	90°	
Θ_d	2°	
A_{Θ_0}/J m^{-2}	1.2×10^{-5}	
A_{Θ_d}/J m^{-2}	5.0×10^{-2}	
d/μm	28.5	[2]
λ/nm	550	[2]

3. Simulation results

The parameters employed in the calculations (unless stated otherwise) are summarized in table 1 and correspond to the nematic, 4-methoxybenzylidene-4′-butylaniline (MBBA).

In the following we will examine the influence of different continuum-model parameters on the optical properties of the HAN cell. In particular, we focus on those parameters which can either be easily varied experimentally (such as the cell thickness) or which are relatively unknown (such as the angle of the easy axis and anchoring coefficient at the homeotropic alignment layer and the flexoelectric coefficient). The latter are the main fitting parameters employed in §4 to model the experimental data obtained by Takahashi *et al.* [2]. Since only the sum of the flexoelectric coefficients appears in the theoretical formalism, we will refer to it as e (i.e. $e=e_{11}+e_{33}$). We note, however, that $e=e_{11}\pm e_{33}$ in the sign convention of Meyer [16] [as, for example, embodied in equation (1)] corresponds to $e=e_{11}\mp e_{33}$ in the convention of Rudquist *et al.* [17].

3.1. *Variation of the cell thickness d*

The top (bottom) panel of figure 1 shows the calculated optical phase difference $\Delta\phi$ (optical transmittance T) as a function of applied d.c. voltage V for various cell thicknesses d. Since the dielectric anisotropy of MBBA is negative, the coupling of the molecular dipoles with the electric field tends to decrease the director tilt angle Θ with increasing magnitude of the applied voltage V, which in turn increases the optical phase difference $\Delta\phi$. Superimposed on the quadratic dielectric effect is the linear flexoelectric effect [see equation (2)], which leads to different slopes of $\Delta\phi$ for positive and negative voltages. Eventually, however, the increasing elastic torque leads to a saturation of $\Delta\phi$ for large values of V. In addition, the flexoelectric effect gives rise to a voltage shift of the curves with respect to the zero applied voltage axis (by $\approx+0.5$ V for the system of figure 1; see bottom panel). This voltage shift is discussed in more detail in §3.5.

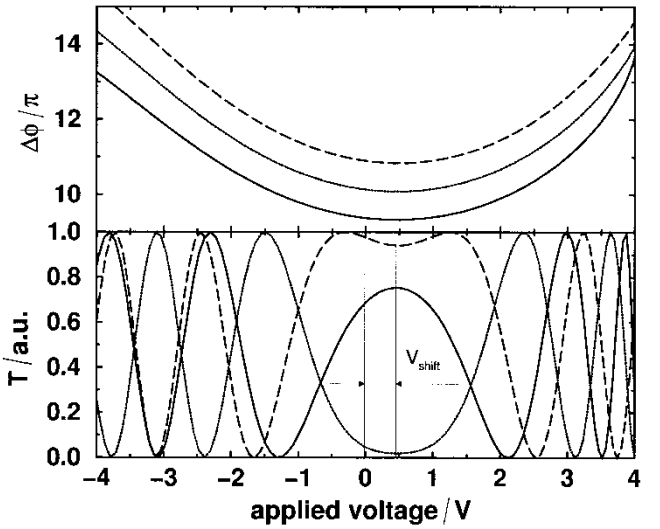

Figure 1. Phase difference $\Delta\phi$ and transmittance T versus applied voltage for the HAN cell of table 1. The cell thicknesses d are 24 μm (full line), 26 μm (dotted line) and 28 μm (dashed line). The voltage shift V_{shift} is shown schematically.

As can be seen from figure 1 (top panel), varying d has a significant influence on $\Delta\phi$ for all voltages, which arises mainly because the HAN cell operates as a variable wave-plate device, i.e. increasing the cell thickness increases the optical path difference between the ordinary and extraordinary ray of normally incident light. Since the device is placed between crossed polarizers, it can be operated as a variable intensity device, i.e. optical phase differences of $\Delta\phi=0$, 2π, 4π, … correspond to $T=0$, phase differences of $\Delta\phi=\pi$, 3π, 5π, … correspond to $T=1$, and intermediate phase differences correspond to intermediate values of T. The latter is illustrated by the bottom panel of figure 1, which shows the optical transmittance curves corresponding to the $\Delta\phi$ curves of the top panel. As can be seen, changing d affects mainly the magnitude and shape of the central peak (at $V\approx+0.5$ V) as well as the number and location of the satellite peaks.

As a consequence of the HAN cell mode of operation (i.e. the variable phase difference combined with the crossed polarizers), it is possible to control the behaviour of the central region of the transmittance curve by an appropriate choice of the cell thickness (i.e. a maximum or minimum of the transmittance at zero applied voltage can be selected). Furthermore, since the

dielectric anisotropy of MBBA is relatively small, the $\Delta\phi$–V curves are quite shallow and a good grey-scaling behaviour of the HAN cell can be achieved (rather than the typical switching-type response of, for example, supertwisted nematic cell devices [1]).

3.2. *Variation of the homeotropic anchoring coefficient* A_{Θ_0}

The top and bottom panels of figure 2 show the corresponding curves of $\Delta\phi$ and T versus V for various values of the anchoring coefficient A_{Θ_0} at the homeotropic alignment layer. As can be seen, for large anchoring coefficients the resulting $\Delta\phi$–V curves are symmetric with respect to the central minimum (see, for example, the curve for $A_{\Theta_0} = 1 \times 10^{-4}\,\mathrm{J\,m^{-2}}$). However, reducing the anchoring coefficient (to values below$\approx 2 \times 10^{-5}\,\mathrm{J\,m^{-2}}$) gives rise to an asymmetry in the phase difference and transmittance curves. The latter can be attributed to the flexoelectric effect as well as the behaviour of the liquid crystal molecules adjacent to the homeotropic alignment layer; i.e. without a strong anchoring to maintain their angle close to 90° the electric field can easily tilt the molecular dipoles at the homeotropic alignment layer. The smaller the homeotropic anchoring coefficient, the easier this becomes. With regard to the flexoelectric effect, we note that negative values of e affect mainly the positive voltage branch of the phase difference and transmittance curves (shown in figure 2), whereas positive values of e affect mainly the negative voltage branch (see figure 5 later). In addition, the bottom panel of figure 2 demonstrates that the voltage shift of the T–V curve depends strongly on A_{Θ_0}. We will return to this point in § 3.5.

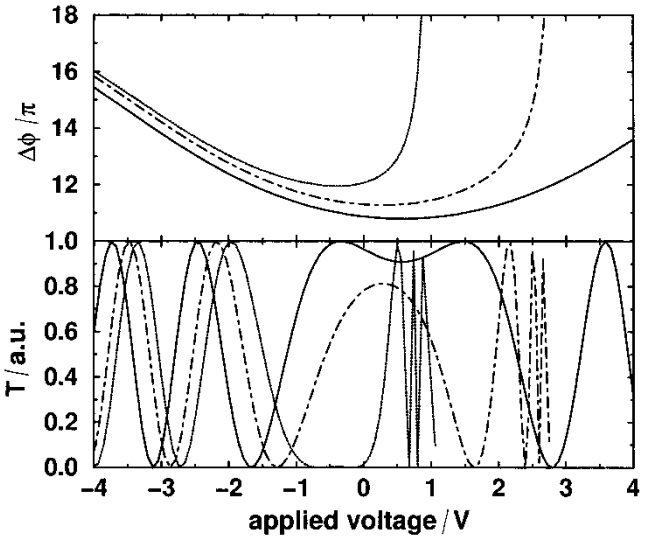

Figure 2. Phase difference $\Delta\phi$ and transmittance T versus applied voltage for the HAN cell of table 1. The homeotropic anchoring coefficients A_{Θ_0} are $1 \times 10^{-4}\,\mathrm{J\,m^{-2}}$ (full line), $6 \times 10^{-6}\,\mathrm{J\,m^{-2}}$ (dot-dashed line) and $2 \times 10^{-6}\,\mathrm{J\,m^{-2}}$ (dotted line).

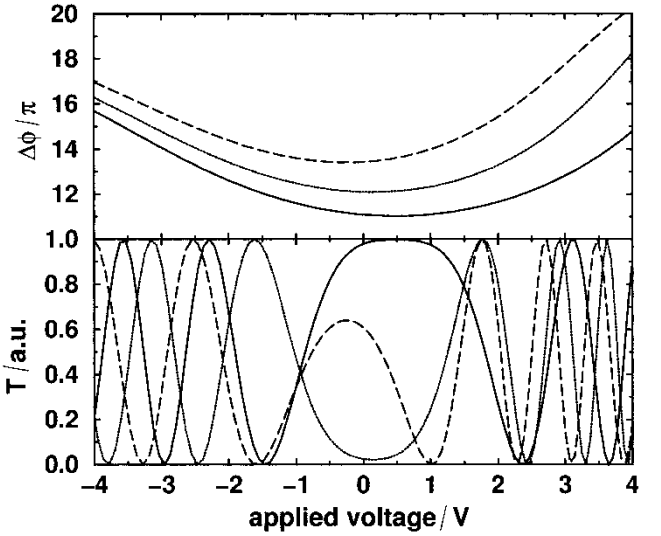

Figure 3. Phase difference $\Delta\phi$ and transmittance T versus applied voltage for the HAN cell of table 1. The angles of the easy axis at the homeotropic alignment layer Θ_0 are 90° (full line), 80° (dotted line) and 70° (dashed line).

3.3. *Variation of the angle of the easy axis at the homeotropic alignment layer* Θ_0

The effect of changing the value of the angle of the easy axis at the homeotropic alignment layer, Θ_0, on $\Delta\phi$ and T is shown in figure 3. As Θ_0 is changed from 90° to 70° the phase difference between the ordinary and extraordinary rays increases for all voltages (see top panel of figure 3). However, this is most noticeable for the positive voltage branch and the central region of the $\Delta\phi$ curves, which strongly affects the optical transmittance of the HAN cell for small voltages. Decreasing the value of Θ_0 also influences significantly the voltage shift induced by the flexoelectric effect. For instance in figure 3, the decrease of Θ_0 is accompanied by a decrease in the voltage shift, which eventually even changes sign from positive to negative values.

3.4. *Variation of the flexoelectric coefficient e*

Figure 4 shows the effect of varying the flexoelectric coefficient $e(=e_{11}+e_{33})$ on the optical response of the HAN cell. The main effect of varying e is to give rise to a voltage shift of the transmittance curves. Negative values of e shift the transmittance curve in the direction of positive voltages and *vice versa*. In contrast, the actual asymmetry of the T–V curves (with respect to the

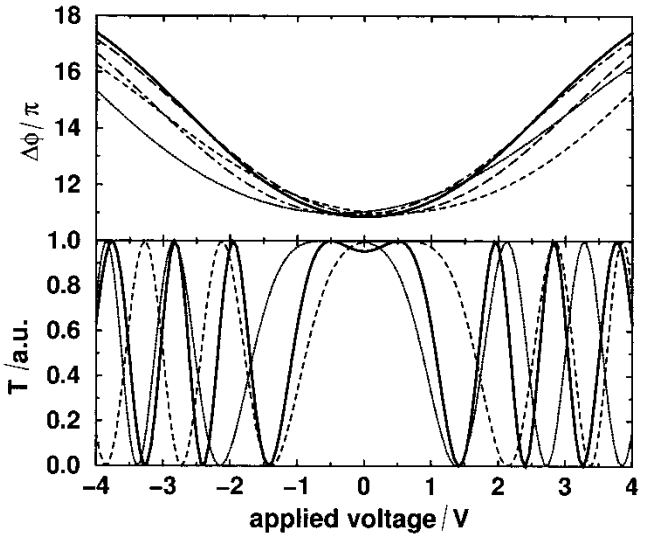

Figure 4. Phase difference $\Delta\phi$ and transmittance T versus applied voltage for the HAN cell of table 1 $(A_{\Theta_0} = 1.2 \times 10^{-5}\,\mathrm{J\,m^{-2}})$ The flexoelectric coefficients e are $-4 \times 10^{-11}\,\mathrm{C\,m^{-1}}$ (dashed line), $-2 \times 10^{-11}\,\mathrm{C\,m^{-1}}$ (long-dashed line), 0 (full line), $+2 \times 10^{-11}\,\mathrm{C\,m^{-1}}$ (dot-dashed line) and $+4 \times 10^{-11}\,\mathrm{C\,m^{-1}}$ (dotted line). (For clarity, only the transmittance curves for $e = 0$ and $\pm 4 \times 10^{-11}\,\mathrm{C\,m^{-1}}$ are shown.)

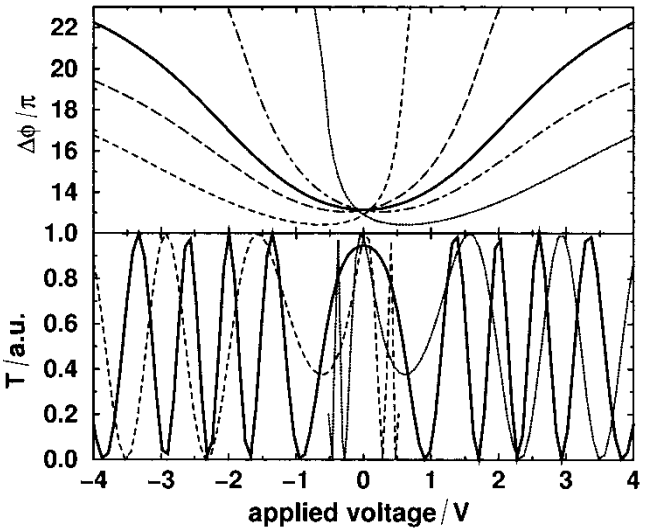

Figure 5. Phase difference $\Delta\phi$ and transmittance T versus applied voltage for the HAN cell of table 1 $(A_{\Theta_0} = 1.2 \times 10^{-6}\,\mathrm{J\,m^{-2}})$. The flexoelectric coefficients e are $-4 \times 10^{-11}\,\mathrm{C\,m^{-1}}$ (dashed line), $-1 \times 10^{-11}\,\mathrm{C\,m^{-1}}$ (long-dashed line), 0 (full line), $+1 \times 10^{-11}\,\mathrm{C\,m^{-1}}$ (dot-dashed line) and $+4 \times 10^{-11}\,\mathrm{C\,m^{-1}}$ (dotted line). (For clarity, only the transmittance curves for $e = 0$ and $\pm 4 \times 10^{-11}\,\mathrm{C\,m^{-1}}$ are shown.)

central minimum or maximum) induced by the flexoelectric effect is rather small. This arises from the fact that, for the calculations shown in figure 4, the anchoring coefficient A_{Θ_0} is relatively large $(1.2 \times 10^{-5}\,\mathrm{J\,m^{-2}})$. As discussed in § 3.2, the homeotropic anchoring coefficient plays an important role in determining exactly how e influences the transmittance curves. This is further illustrated by figure 5, which shows the optical response of the HAN cell corresponding to figure 4, except for a smaller value of the homeotropic anchoring coefficient $A_{\Theta_0} = 1.2 \times 10^{-6}\,\mathrm{J\,m^{-2}}$. As can be seen, the asymmetry induced by the flexoelectric effect in this case in much more pronounced than, for example, in figure 4. However, it has to be noted that in the absence of *any* flexoelectric contribution the transmittance curves are always *symmetric* with respect to the zero applied voltage axis.

3.5. *The e-dependent voltage shift*

An important aspect of HAN cells (scientifically rather than technologically) is their use in determining the values of the flexoelectric coefficients. Takahashi *et al.* [2] demonstrated that the in-plane electric field HAN cell can be used to find the value of $e_{11} - e_{33}$, whereas a HAN cell with the electric field applied along the cell normal can be used to find the value of $e_{11} + e_{33}$ (the value we refer to as e). The combination of these two experiments would, therefore, enable the determination of e_{11} as well as e_{33}.

In particular, Takahashi *et al.* [2] argued that a comparison between the measured and the calculated voltage shift of the transmittance curve (defined as V_{shift} in figure 1) can be used to determine the value of e. We have utilized our present continuum model to calculate the e-dependent voltage shift, and the results of the calculations are shown in figure 6 for different homeotropic anchoring coefficients A_{Θ_0}. As can be seen from this figure, when the anchoring coefficient is high the relationship between e and V_{shift} is linear, and the constant of proportionality is unchanged for a large range of anchoring coefficients (i.e. for $A_{\Theta_0} \gtrsim 20 \times 10^{-6}\,\mathrm{J\,m^{-2}}$). However, when the anchoring coefficient is lowered the gradient of the V_{shift} versus e curve becomes initially smaller, eventually reverses its sign and the linearity is lost. Indeed, certain values of the anchoring coefficient give rise to a non-monotonic relationship between e and V_{shift}, i.e. e is no longer uniquely defined in terms of the voltage shift. This can be seen, for example, from the curve for $A_{\Theta_0} = 4 \times 10^{-6}\,\mathrm{J\,m^{-2}}$ in figure 6, i.e. two different values of e can give rise to the same voltage shift. Consequently, the method proposed by Takahashi *et al.* [2] to determine e is not viable for low homeotropic anchoring coefficients, and even for high homeotropic anchoring coefficients it may be problematic if the angle

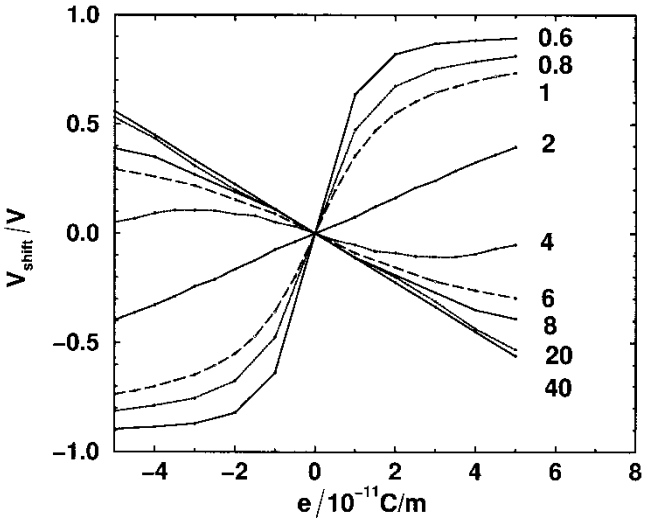

Figure 6. Voltage shift V_{shift} versus flexoelectric coefficient e for the HAN cell of table 1. The curves are labelled with the values of the homeotropic anchoring coefficients A_{Θ_0} in units of $10^{-6}\,J\,m^{-2}$.

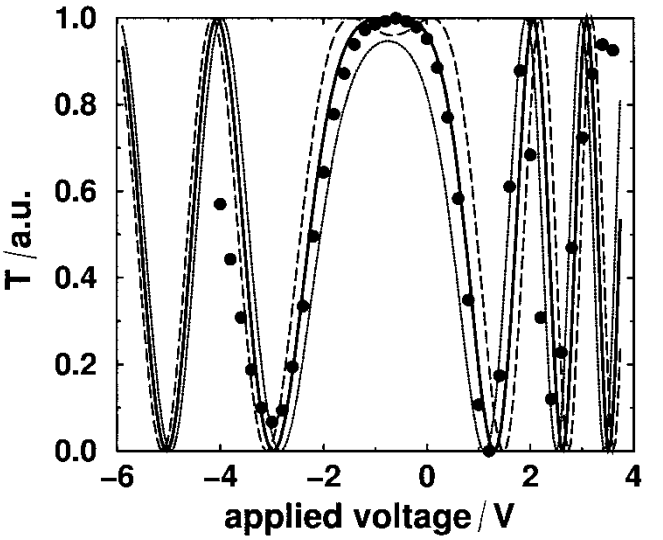

Figure 8. Transmittance versus applied voltage for different values of the angle of the easy axis at the homeotropic alignment layer: $\Theta_0 = 76°$ (dotted line), 77° (solid line, best fit) and 78° (dashed line). A_{Θ_0} and e are equal to their best-fit values, $4.5 \times 10^{-6}\,J\,m^{-2}$ and $-2.0 \times 10^{-11}\,C\,m^{-1}$, respectively. Full circles: experimental data [2].

of the easy axis at the homeotropic alignment layer is unknown. In this respect, it has to be noted that the asymmetry in the experimental transmittance curve (observed by Takahashi *et al.* [2] and shown by the full circles in figures 7 to 9) indicates that the anchoring coefficient at the homeotropic alignment layer is indeed low. This would be a plausible explanation for the large variations in the published values of e for MBBA [2]. The alternative is, of course, to model the entire optical response of the HAN cell (rather than just V_{shift}). We will address this point in the following section.

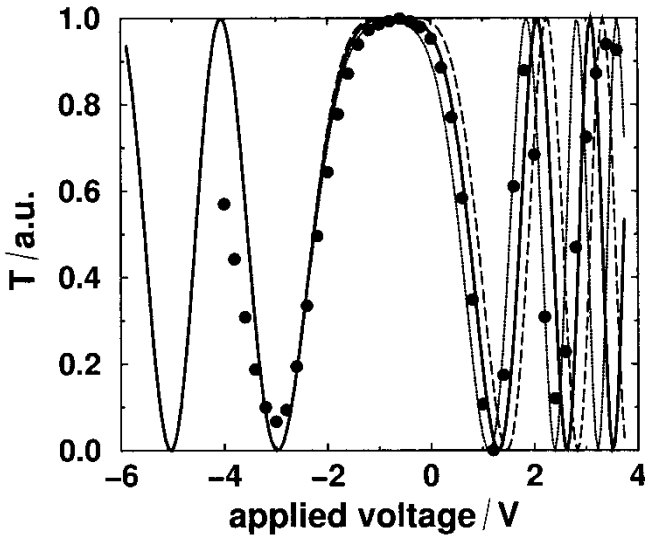

Figure 7. Transmittance versus applied voltage for different values of the homeotropic anchoring coefficient: $A_{\Theta_0} = 4.0 \times 10^{-6}\,J\,m^{-2}$ (dotted line), $4.5 \times 10^{-6}\,J\,m^{-2}$ (solid line, best fit) and $5.0 \times 10^{-6}\,J\,m^{-2}$ (dashed line). Θ_0 and e are equal to their best-fit values, 77° and $-2.0 \times 10^{-11}\,C\,m^{-1}$, respectively. Full circles: experimental data [2].

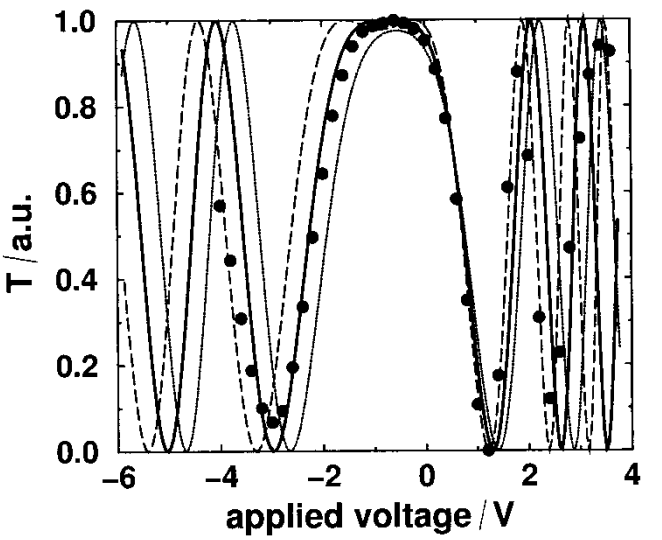

Figure 9. Transmittance versus applied voltage for different values of the flexoelectric coefficient: $e = -1.5 \times 10^{-11}\,C\,m^{-1}$ (dotted line), $-2.0 \times 10^{-11}\,C\,m^{-1}$ (solid line, best fit) and $-2.5 \times 10^{-11}\,C\,m^{-1}$ (dashed line). A_{Θ_0} and Θ_0 are equal to their best-fit values, $4.5 \times 10^{-6}\,J\,m^{-2}$ and 77°, respectively. Full circles: experimental data [2].

4. Comparison with experiment

We will now compare the results of our calculations with the experimental observations of Takahashi *et al.* [2]. Details of the sample preparation and the experimental procedure can be found elsewhere [2]. Briefly, one of the substrates was coated with a polyimide film and treated by rubbing to induce homogeneous alignment. The other substrate was coated with another type of polyimide film to induce homeotropic alignment. The HAN cell was filled with the nematic liquid crystal MBBA, the measurements were carried out at a temperature of 30°C and the wavelength of the light beam was 550 nm.

The experimental transmittance–voltage data obtained by Takahashi *et al.* is shown by the full circles in figures 7 to 9. In these figures we have scaled the experimental data to lie between $T=0$ and 1 in order to account for absorption and scattering of the light beam by the various HAN cell layers. In view of our findings described in § 3, we are readily able to deduce certain properties of the experimental system. For instance, (1) the asymmetry in the experimental T–V curve leads us to conclude that the homeotropic anchoring coefficient is relatively small, (2) the observed asymmetry also indicates a non-zero contribution of the flexoelectric effect and (3) the nature of the asymmetry (i.e. the positive voltage branch is much more affected than the negative voltage branch) indicates that the sign of the flexoelectric coefficient e is negative.

Figures 7 to 9 also show the calculated T–V curves for small variations of the fitting parameters about their best-fit values: $A_{\Theta_0}=(4.5\pm0.5)\times10^{-6}\,\mathrm{J\,m^{-2}}$ (figure 7), $\Theta_0=77^\circ\pm1^\circ$ (figure 8) and $e=(-2.0\pm0.5)\times10^{-11}\,\mathrm{C\,m^{-1}}$ (figure 9). The effects of these small variations essentially reflect the findings described in § 3, namely A_{Θ_0} only affects the positive voltage branch (for negative e), the voltage shift and central region of the T–V curve is very sensitive to changes in Θ_0, and e has a pronounced influence on the asymmetry of the T–V curve. The best-fit is represented by the full line in figures 7 to 9. As can be seen, for low voltages the agreement between the calculations and the experimental data of Takahashi *et al.* [2] is very good. The discrepancy between theory and experiment increases for higher voltages, which could be due to internal reflections at the interfaces as well as uncertainties in the experimental data and in the fitting parameters.

The fitting parameters e and A_{Θ_0} are listed in table 2, together with the parameters obtained by Takahashi *et al.* [2], Ponti *et al.* [6], Madhusudana and Durand [8] and Valenti *et al.* [18]. As can be seen, the flexoelectric coefficient obtained using the present model has the same sign but is significantly smaller than the Takahashi value. Similarly, the present model indicates that the anchoring strength of MBBA at the homeotropic polyimide alignment layer is much smaller than previously reported [2]. It is interesting to note, however, that our values of e and A_{Θ_0} agree remarkably well with the values obtained by Madhusudana and Durand [8] and by Valenti *et al.* [18] for MBBA on a homeotropic silane alignment layer. With regard to the results of Ponti *et al.* [6], we note that these authors re-analysed the experimental data of Madhusudana and Durand [8] in a self-consistent calculation by taking the influence of charged impurities into account. Both Ponti *et al.* [6] and Madhusudana and Durand [8] assume infinite anchoring strength at the homogeneous alignment layer and employ a one-constant approximation. However, at present we have no plausible explanation for the large discrepancy between the value of e obtained by Ponti *et al.* [6] and the other values listed in table 2.

Table 2. Continuum-model parameters e and A_{Θ_0} employed to fit the experimental data of Takahashi *et al.* [2] ($\Theta_0=77^\circ$, $\Delta\varepsilon=-0.22$, $\Delta n=0.23$, $d=28.5\,\mu\mathrm{m}$ [2, 6]; HAL: homeotropic alignment layer). The parameters obtained by Takahashi *et al.* [2], Ponti *et al.* [6], Madhusudana and Durand [8] and Valenti *et al.* [18] are listed for comparison.

Origin (ref)	HAL	$e/10^{-11}\,\mathrm{C\,m^{-1}}$	$A_{\Theta_0}/10^{-6}\,\mathrm{J\,m^{-2}}$
Best fit	polyimide	−2.0	4.5
[2]	polyimide	−5.4	100
[6]	silane	+8.8	16
[8]	silane	−2.5	3.6
[18]	silane	−1.5	5.8

5. Conclusion

A continuum model was employed to study systematically the optical response of hybrid-aligned nematic (HAN) liquid crystal cells under the application of an external electric field. The flexoelectric effect was included in the simulations. The main findings were: (1) variations in the cell thickness can be employed to select the behaviour of the HAN cell at zero applied voltage; (2) the interplay between the flexoelectric effect and the anchoring strength at the homeotropic alignment layer is of paramount importance to the optical response of the cell; (3) the flexoelectric effect leads to a voltage shift of the transmittance curve; (4) the flexoelectric effect can also give rise to an asymmetry in the transmittance curve; (5) the sign of the flexoelectric coefficient determines which voltage branch experiences the asymmetry in the optical response (i.e. the positive voltage branch for negative flexoelectric coefficients and *vice versa*); (6) the extent of the asymmetry is mainly determined by the homeotropic anchoring coefficient; however, (7) in the

absence of a flexoelectric effect, the optical response is always symmetric with respect to the zero applied-voltage axis. It was also demonstrated that, with an appropriate choice of material and cell parameters, HAN cells can be designed which exhibit good grey-scaling behaviour.

The model was then applied to the experimental system of Takahashi *et al.* [2] and the following parameters were obtained from the fitting procedure: the anchoring coefficient for MBBA at a homeotropic polyimide alignment layer $A_{\Theta_0} = (4.5 \pm 0.5) \times 10^{-6}\,\mathrm{J\,m^{-2}}$, the easy-axis angle at the homeotropic alignment layer $\Theta_0 = 77^\circ \pm 1^\circ$ and the flexoelectric coefficient $e = (-2.0 \pm 0.5) \times 10^{-11}\,\mathrm{C\,m^{-1}}$.

N. T. K. would like to thank the EPSRC for the award of a research studentship.

References

[1] Blinov, L. M., and Chigrinov, V. G., 1994, *Electro-optic Effects in Liquid Crystal Materials* (New York: Springer), Chap. 8.
[2] Takahashi, T., Hashidate, S., Nishijou, H., Usui, M, Kimura, M., and Akahane, T., 1998, *Jpn. J. appl. Phys. 1*, **37,** 1865.
[3] Warrier, S. R., and Madhusudana, N. V., 1997, *J. Phys. II Fr.*, **7,** 1789.
[4] Toyooka, T., Yoda, E., Yamanashi, T., and Kobori, Y., 1999, *Displays*, **20,** 221.
[5] Hong, S. H., Kim, H. Y., Kim, J. H., Nam, S. H., Lee, M. H., and Lee, S. H., 2002, *Jpn. J. appl. Phys. 1*, **41,** 4571.
[6] Ponti, S., Ziherl, P., Ferrero, C., and Žumer, S., 1999, *Liq. Cryst.*, **26,** 1171.
[7] Maheswara Murthy, P. R., Raghunathan, V. A., and Madhusudana, N. V., 1993, *Liq. Cryst.*, **14,** 1107.
[8] Madhusudana, N. V., and Durand, G., 1985, *J. Physique Lett.*, **46,** L195.
[9] Barbero, G., Taverna-Valabrega, P., Bartolino, R., and Valenti, B., 1986, *Liq. Cryst.*, **1,** 483.
[10] Blinov, L. M., Barnik, M. I., Ohoka, H., Ozaki, M., and Yoshino, K., 2001, *Jpn. J. appl. Phys. 1*, **40,** 5011.
[11] Blinov, L. M., Barnik, M. I., Ozaki, M., Shtykov, N. M., and Yoshino, K., 2000, *Phys. Rev. E*, **62,** 8091.
[12] Yang, F., Ruan, L., and Sambles, J. R., 2000, *J. appl. Phys.*, **88,** 6175.
[13] Mazzulla, A., Ciuchi, F., and Sambles, J. R., 2001, *Phys. Rev. E*, **64,** 021708.
[14] Jewell, S. A., and Sambles, J. R., 2002, *J. appl. Phys.*, **92,** 19.
[15] Barbero, G., and Evangelista, L. R., 2001, *An Elementary Course on the Continuum Theory for Nematic Liquid Crystals* (Singapore: World Scientific), Chap. 3.6.
[16] Meyer, R. B., 1969, *Phys. Rev. Lett.*, **22,** 918.
[17] Rudquist, P., Komitov, L., Lagerwall, S. T., 1994, *Phys. Rev. E*, **50,** 4735; Rudquist, P., and Lagerwall, S. T., 1997, *Liq. Cryst.*, **23,** 503.
[18] Valenti, B., Bertoni, C., Barbero, G., Taverna-Valabrega, P., and Bartolino, R., 1987, *Mol. Cryst. liq. Cryst.*, **146,** 307.